Advances in Science and Technology Research Journal

Advances in Science and Technology Research Journal, 2026, 20(4), 359–372
https://doi.org/10.12913/22998624/215406
ISSN 2299-8624, License CC-BY 4.0

Received: 2025.11.24
Accepted: 2026.02.06
Published: 2026.03.01

Dynamic modeling and response of deep mine hoisting systems considering distributed-mass viscoelastic ropes

Sy Nam Nguyen[1], Duc Hieu Tran[2*]

[1] Faculty of Civil and Industrial Construction, Hanoi University of Civil Engineering, No. 55 Giai Phong Street, Bach Mai Ward, Hanoi City, Vietnam
[2] Faculty of Mechanical Engineering, Hanoi University of Civil Engineering, No. 55 Giai Phong Street, Bach Mai Ward, Hanoi City, Vietnam
* Corresponding author's e-mail: hieutd@huce.edu.vn

ABSTRACT

The article deals with the problem of a dynamic processes in mine hoisting systems critically affecting operational safety and performance. Existing models often treat ropes as weightless viscoelastic elements, neglecting the combined effects of rope deformation, distributed mass, material stiffness, and balancing ropes, which are increasingly significant at high lifting heights. This study presents a simplified yet comprehensive modeling approach: the rope is divided into equal segments with distributed mass, each represented as a discrete mass connected by weightless viscoelastic elements. This method captures the interactions of elasticity, damping, and distributed mass while remaining computationally efficient. Simulation results demonstrate improved prediction of rope deformation and dynamic responses under various operational conditions. The proposed approach provides practical insights for the design, optimization, and safe operation of deep mine hoisting systems, addressing the limitations of previous models and supporting enhanced reliability in high-risk lifting operations.

Keywords: shaft hoisting, dynamics, rope, mass distribution, Lagrange's equations.

INTRODUCTION

Modeling the dynamics of mine hoisting systems is highly complex and requires consideration of multiple factors during model development. These factors include both the primary and auxiliary components of the hoist, as well as the entire system, encompassing most of the relevant forces and masses.

Reutov et al. [1] demonstrated that the loaded block pulley model could be incorporated as a subsystem in the dynamic computer model of a lifting crane. This is achieved by using the subsystem output parameters to execute the axial force on the upper block pulley, the movement of the exit rope section, and the rope tension force at this section. Ilin et al. [2] presented the dependence of dynamic parameters, which determine the risk of emergency situations, on the technical state parameters of individual parts of the winding plant. The authors rely on comprehensive studies of the structure of the mine winding mill, which is considered a repetitive, discrete-continuous system with many deviations of operating parameters from the expected values.

Ilin et al. [3] presented an analysis of the state of the profiles of conductors in mine shafts with a long service life. A solid model of barrel reinforcement, along with the results of calculations and the distribution of stress concentration along the length of the shot, were provided. The results of measuring the dynamic parameters of the vessel-reinforcement systems under the conditions of active shafts were also presented.

Shebela and Pavelek [4] analyzed and demonstrated that the dynamics of the drive system do not affect the dynamics of the entire system. The dynamics of the bypass process are influenced primarily by the position of the guide shaft sections (their deformation and deviation from

the vertical) and by the condition of the rollers in coordination with the axis of guide rods.

Ilin et al. [5] showed that dynamic processes in mine hoisting installations, in both operating and transition modes, exhibit strong interconnectedness and cumulative strengthening of risk-forming phenomena in "lifting vessel – reinforcement" systems. The cumulative effect can occur when critical processes are interrelated in different units of a hoisting machine, even when the parameters of each process do not exceed permissible limits.

Kaczmarczyk and Ostachowicz [6] introduced a simulation model to investigate the dynamic response of a deep mine hoisting cable system during a winding cycle. Specifically, the lateral motions of the catenary cable and the longitudinal motion of the vertical rope with conveyance are observed on a fast time scale. Additionally, a slow time scale is introduced to monitor the variation of slowly varying parameters of the system.

Ma and Xiao [7] presented a study to determine the appropriate lifting parameters of a multi-rope friction mining winch. A dynamic model was established and experimentally validated, exploring the dynamic characteristics of both constant-length lifting chains and variable-length vertical lifting chains, each subjected to a defined external periodic excitation caused by the oscillation of the head pulley.

Chaplin [8] provided a physical model of the deterioration of lifting ropes through laboratory testing. Carefully managed service tests can safely explore the impact of certain changes to operational variables, enabling deeper level operations. However, such an approach cannot assess the effects of increased differential torsional strain associated with increasing suspension length. Khoreshok et al. [9] proposed calculations to optimize the load of the winch (lift) for different usage modes. These calculations can be used to construct brake lifts with new designs.

Zhang et al. [10] studied the dynamic torsional characteristics of a mine lifting rope and its internal helical parts. They developed theoretical models of torque, unit helix angle, torsion angle, torsion parameters, and torsion stress to investigate the dynamic torsion characteristics of the lifting rope and its internal helical parts under the action of drag. The results show three-phase fluctuation trends in wire tension and torque.

Yao et al. [11] studied the influence of drum winding on the impact response of superdeep mine hoisting systems. The hoisting velocity and acceleration are accurately modeled and calculated according to the cable groove structure of the LeBus drum. The impact responses of displacement and dynamic load are obtained by applying the established model. This study provided valuable technical support for the design and optimization of mine winches in ultra-deep mines.

Wang et al. [12] established a nonlinear dynamic model of the coal mine hoisting system using the Hamilton principle. The nonlinear partial differential equations of the coal mine hoisting system were discretized into ordinary differential equations by fourth-order Galerkin truncation. The research results show that the axial vibration displacement of a constant-length cable is one order of magnitude smaller than that of a variable-length cable. The load has the greatest influence on the axial vibration displacement of the hoisting cable, while speed has the least influence on the axial vibration displacement of the hoisting cable.

Cao et al. [13] presented a study the tension and torsion characteristics of ropes. Three-node elements in the transformation domain of the string were used, and the corresponding differential algebraic equations (DAEs) were derived using Lagrange equations of the first kind. The dynamic equations, originally in DAE form, were transformed into ordinary differential equations (ODEs). The dynamic responses of tension, torsion, and acceleration were analyzed based on the drum radius error, showing that drive misalignment between the ropes can have a significant influence on the tension difference, potentially causing one of the ropes to go slack. To design and manufacture the drum in the ultra-deep parallel hoisting system, it is crucial to control the unreasonable difference between the ropes.

Wolny and Matachowski [14] determined the interaction force between the steel structure and the conveyor belt, as well as the stress on the carrying parts, based on the kinematic analysis of the hoist operation. Their analysis took into account irregularities or deflections of the guide wire and their random occurrence. Several tests on real objects were performed to validate the correctness of the model.

Kaczmarczyk and Ostachowicz [15] used a classical motion coordinate frame and Hamilton's principle to develop a mathematical model with distributed parameters to study the dynamic behavior of deep mine hoisting cables. The model described the horizontal and vertical dynamics of the cable according to a nonlinear

partial differential equation consistent with the non-stationary nature of the system, using the Rayleigh–Ritz process to build a discrete mathematical model. A coupled system of non-stationary nonlinear second-order differential equations governs the transient state of the cable system. This discrete model, with second- and third-order nonlinear terms, describes the modal interactions between the horizontal vibrations of the catenary and the vertical vibrations of the vertical string. It shows that the response of the vertical catenary system may exhibit some resonance phenomena. The parameters of a typical deep mine coil winding machine are used to determine the depth position of the resonant regions in increasing cycles with different winding velocities.

Yao and Xiao [16] studied the impact of lifting loads on the horizontal vibration of hoisting wire rope systems during lifting in coal mines. They carried out a dynamic analysis of vertical hoisting wire ropes and performed dynamic simulations to examine the effects of lifting loads on horizontal vibrations. The results showed that under the second-order excitation frequency, a large non-uniform horizontal amplitude was excited when the lifting load was between 0 and 5000 kg. This could lead to collisions between adjacent wire rope systems and accelerate wire rope breakage. This study will greatly assist in facility maintenance, machinery design, and the technical optimization of floor-type multi-rope friction mine hoists.

Wang et al. [17] investigated the lateral response of a moving lifting vehicle within a cable-guided lifting system. The equivalent mass and stiffness of the guide cable, along with the motion equations, were formulated based on the Hamilton principle, utilizing the Galerkin method to convert the governing equations into a set of ordinary differential equations. An ADAMS simulation model with multiple degrees of freedom was developed to validate the theoretical model. The numerical solution for the set of equations was obtained using the Newmark-β method, and the convergence of the solution was examined. The results indicated that the numerical simulations were in strong agreement with the ADAMS simulations, and the presented model was consistent with previous models. The influence of parameters on the lateral response was analyzed, revealing that the maximum lateral displacement was linearly proportional to the excitation amplitude.

Yao et al. [18] analyzed and optimized key lifting parameters by examining the multi-source coupled vibration characteristics of lifting chains. Using an established theoretical model, they explored these vibration characteristics. The proposed optimization methods provided new constraints that can be used to determine the optimal lifting parameters during the design or maintenance of floor-type multi-wire friction mine hoists.

Lu et al. [19] investigated the impact of uncertain structural parameters on the reliability of a main-shaft device. They conducted a probabilistic optimization design based on parameter sensitivity results and performed random response analysis through experiments. To evaluate the reliability of the device under uncertain parameters, they employed the moment-based saddle point approximation method. The sensitivity analysis revealed that the torque and contact length of the left bearing had a significantly greater impact on the structural reliability of the main-shaft device compared to other variables.

Guo et al. [20] studied the nonlinear dynamic response of wire ropes under periodic excitation in a friction winch system and conducted longitudinal excitation experiments with varying periodic excitation frequencies. They analyzed the nonlinear dynamic characteristics of the wire rope, including transverse, longitudinal, and coupled vibrations, using time-frequency analysis. The results showed that transverse vibrations were forced vibrations following excitation, while longitudinal vibrations exhibited complex and random states. At certain excitation frequencies, the amplitudes and vibration intensities deviated significantly from their linear trends, indicating superharmonic resonances and typical nonlinear multi-order natural frequency characteristics. The lifting motion introduced additional high-order harmonic ripples, leading to fundamental wave distortion at low-frequency excitation. The experiments also revealed the coupling characteristics of transverse-longitudinal wire rope vibrations during lifting.

Guo et al. [21] investigated the dynamics of longitudinal wire ropes in friction lifting systems and their coupling effect on friction transmission. Using an established simulation model, they analyzed the dynamics of both the wire rope and the friction transmission. The vibration of the longitudinal wire rope was represented as a random disturbance. The study found that a decrease in the friction coefficient increases the slip between the wire rope and the liner, which helps to narrow down the dynamic tension mode. Conversely, an

increase in the vibration of the longitudinal wire rope reduces the friction force between the wire rope and the liner.

Peterka et al. [22] analyzed the rope sample and demonstrated that a combination of multiple factors contributed to its failure. Several issues can affect the service life of a wire rope, including poor-quality input materials, mixing wires of different strength grades in the rope structure, improper reeving into the hoist system, incorrect operation, or selecting a rope design unsuitable for the working conditions. During the operation of the cargo cableway, the hauling rope was damaged within a very short period of time. These issues indicate that mechanical testing of rope properties prior to deployment is essential. Several customers have already adopted this procedure, and the results show a significant improvement in operational safety as well as a reduction in failures and complaints associated with low-quality ropes.

Peterka et al. [23] conducted tests on crane steel wire ropes with a separate core using non-destructive testing (NDT) methods. Conventional visual inspection proved ineffective for the ropes with this structural configuration. On the basis of practical experience, the authors observed that surface cracks often appear after the internal strands begin to deteriorate, which may eventually lead to rope failure during operation. Reducing the pulley diameter can also cause multi-axis bending of the rope, increasing fatigue stresses due to friction between the strands. Similar stress conditions arise when the rope end is improperly processed. Moreover, excessive use of the crane can create hazardous situations that compromise occupational safety. These findings highlight the need for operators to strictly adhere to safety standards, especially when using new cranes, pulleys, and steel wire ropes.

Kalentev et al. [24] presented a numerical analysis of the stress-strain state of a rope strand, including axial deformation and stress distribution under applied torsional moments. This work provided complementary insight into strand-level torsional effects that may influence aggregate rope dynamics as well as inform about potential extensions of the authors' distributed-mass axial model to include torsion-axial coupling.

Most of the problems related to hoisting mechanism dynamics, as discussed in the aforementioned literature, have been solved using the methods that consider the ropes as weightless viscoelastic elements. The equivalent mass of the rope is determined by the Raynol method, and the rope deformation under dynamic loading is assumed to correspond to its deformation under static loading. The mass of the balanced rope is fully or partially incorporated into the calculation model. However, these models do not simultaneously consider deformation, distributed mass, material resistance and balancing cables. As the lifting height increases, the influence of the distributed mass of the rope on the dynamic processes becomes more significant.

In addition, although several studies have emphasized the importance of lateral-torsional interactions in deep hoisting systems – particularly for the ropes with complex helical structures or under periodic excitation [10, 20] – these effects are not included in the present model. The focus of this work is placed on axial dynamics because, at lifting depths approaching several hundred to nearly one thousand meters, longitudinal deformation, tension variation, and vertical wave propagation dominate the dynamic behavior and operational safety of the system. Incorporating lateral–torsional coupling would introduce additional geometric nonlinearities and multiple degrees of freedom, resulting in a significantly more complex model beyond the intended scope. The present axial formulation provides a computationally efficient foundation that can later be extended to multi-directional coupling in future research.

To simplify the solution of hoisting mechanism dynamics problems, this study proposed a straightforward approach: the rope, with mass distributed along its length, is divided into equal segments and replaced by n masses connected by weightless viscoelastic elements.

Although several prior studies have shown that torsional deformation and torsional–axial coupling may influence rope behavior under certain operating conditions, these effects were not included in the present model. At ultra-deep hoisting depths such as the 930 m considered here, the rope experiences high axial tension, which suppresses torsional deformation and significantly weakens torsion–axial interaction. As a result, torsion contributes only minor modifications to the high-frequency components of the response, while the dominant dynamics remain governed by axial stiffness, distributed mass, and longitudinal wave propagation. The presented formulation therefore focuses on axial dynamics to ensure computational efficiency, while providing a foundation that can be extended to include torsional coupling in future research.

EQUATIONS OF MOTION

The hoist model shown in Figure 1 consists of the following parts: cabin (1), counterweight (2), and the hoist unit (3). The lifting system includes hoisting rope branches 1 and 2, while the balancing system includes tail rope branches 3 and 4. In the hoist model of an elevator used in deep mines, the lifting and lowering ropes are very long (several thousand meters), so the rope weight is significant, and the longitudinal deformation must also be taken into account. Therefore, the rope is considered as a tensioned string with a distributed mass μ_c. At position x_i, the rope elongates by an amount u_i, where i is the index of the rope branch i = 1.2 (Figure 1).

Since the height of the cabin is negligible compared to the length of the rope, the cabin is considered as a concentrated mass. The horizontal oscillations of the objects are neglected. It should be noted that the assumption of negligible horizontal oscillations is valid primarily for deep-shaft hoisting operations. At lifting depths above approximately 600–700 m, the axial tension in the rope becomes sufficiently large that the lateral stiffness increases and transverse displacements remain very small compared to longitudinal deformation. In contrast, for medium-depth systems (300–600 m), reduced rope tension may allow external disturbances or guide-rail irregularities to excite noticeable lateral motion. The assumption becomes unreliable for shallow hoisting operations with rope lengths below about 300–400 m, where low axial tension results in significant lateral flexibility. Since the present study considers a hoisting depth of 930 m, axial dynamics dominate and the omission of horizontal oscillations does not introduce substantial modeling error.

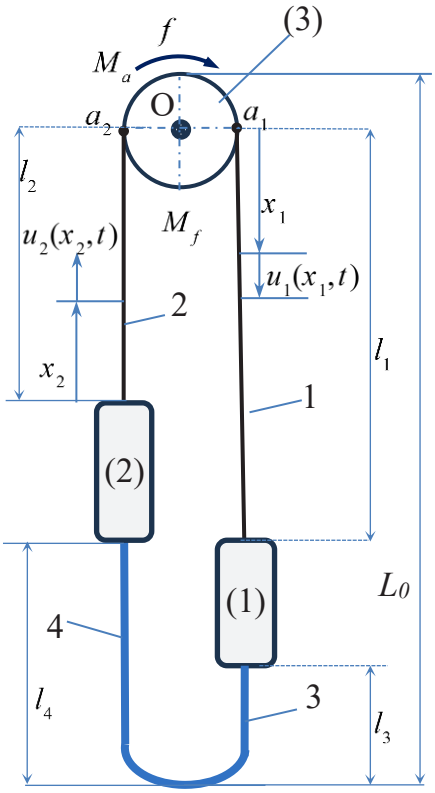

Figure 1. Model of deep mine hoisting systems

*) Consider the rope element dx_1 on branch 1 and the rope element dx_2 on branch 2. At the initial moment, their positions are x_{10}, x_{20}. When the hoist starts moving, the positions of these elements (excluding deformation) are given as:

$$x_1 = x_{10} + R\phi(t), x_2 = x_{20} - x_1 = x_{20} - R\phi(t) \quad (1)$$

where $\phi(t)$ is the rotation angle of the hoist.

The coordinates of those elements including deformation are:

$$x_1^0 = x_1 + u_1(x_1,t); x_2^0 = x_2 + u_2(x_2,t) \quad (2)$$

The velocity of the rope element dx_1:

$$v_1 = \frac{dx_1^0}{dt} = \dot{x}_1 + \dot{u}_1 + u_{1,x}\dot{x}_1 = R\omega + \dot{u}_1 + R\omega u_1' \quad (3)$$

The velocity of cabin (1):

$$V_1 = R\omega + \dot{u}_1(l_1,t) + R\omega u_{1,x}(l_1,t) \quad (4)$$

The velocity of the rope element dx_2:

$$v_2 = \frac{dx_2^0}{dt} = \dot{x}_2 + \dot{u}_2 + u_{2,x}\dot{x}_2 = -R\omega + \dot{u}_2 - R\omega u_2' \quad (5)$$

The velocity of the counterweight (2):

$$V_2 = -R\omega + \dot{u}_2(l_2,t) - R\omega u_{2,x}(l_2,t) \quad (6)$$

where: $u_{i,x} = \partial u_i/\partial x_i, \omega = \partial\phi/\partial t = \dot{\phi}$

Kinetic energy:

$$T = \frac{1}{2}J_3\omega^2 + \frac{1}{2}\rho_c\int_0^{\pi R} V_0^2 dx + \frac{1}{2}\rho_c\int_0^{l_1} v_1^2 dx_1 + \frac{1}{2}\rho_c\int_0^{l_2} v_2^2 dx_2 + \frac{1}{2}m_1V_1^2 + \frac{1}{2}m_2V_2^2 + \frac{1}{2}m_3(x_1,t)V_1^2 + \frac{1}{2}m_4(x_2,t)V_2^2 \quad (7)$$

where: J_3 is the moment of inertia of component (3) about its axis of rotation, $\rho_c$is the mass per unit length of the hoisting rope, and $V_0 = R\omega$ is the longitudinal velocity of the rope segment passing over the hoist drum l_1, l_2 are the lengths of rope branches 1 and 2, respectively; m_1, m_2 are the masses of cabins (1) and counterweight (2), respectively; m_3, m_4 are the masses of the counterweight rope branches 3 and 4, respectively, which are determined by the formula $m_3 = \rho_b l_3, m_4 = \rho_b l_4$, with ρ_b representing the mass per unit length of the counterweight rope.

*) *Elastic potential energy:* Let $T_{10}(x_1)$ and $T_{20}(x_2)$ be the initial static tensions of the rope branches. Since the ropes have mass, these tensions are functions of position. The elastic potential energy is then given by:

$$U_E = \int_0^{l_1} T_{10}(x_1)\frac{\partial u_1}{\partial x_1}dx_1 + \int_0^{l_2} T_{20}(x_2)\frac{\partial u_2}{\partial x_2}dx_2 + \frac{1}{2}EA\int_0^{l_1}\left(\frac{\partial u_1}{\partial x_1}\right)^2 dx_1 + \frac{1}{2}EA\int_0^{l_2}\left(\frac{\partial u_2}{\partial x_2}\right)^2 dx_2 \quad (8)$$

The initial tension is determined based on the static equilibrium equation:

$$T_{10}(x_1) = \left(r_c(l_1 - x_1) + m_1 + r_b l_3\right)g;\ \ T_{20}(x_2) = \left(r_c x_2 + m_2 + r_b l_4\right)g \quad (9)$$

*) *Gravitational potential energy:* Taking the reference point of potential energy at the hoist drum shaft, we have:

$$U_G = -\int_0^{l_1}\rho_c g x_1 dx_1 - \int_0^{l_2}\rho_c g x_2 dx_2 - m_1\left(l_1 + u_1(l_1,t)\right)g - m_2\left(l_2 + u_2(l_2,t)\right)g$$
$$-\rho_b l_3 g\left(l_1 + u_1(l_1,t) + \frac{l_3}{2}\right) - \rho_b l_4 g\left(l_2 + u_2(l_2,t) + \frac{l_4}{2}\right) \quad (10)$$

*) *Virtual work:*

$$\delta W = \left(M_a - M_f\right)\delta\phi \quad (11)$$

where: M_a, M_f are, respectively, the total driving torque and the total resisting torque applied to the hoist drum shaft.

*) *Energy dissipation function* due to viscous damping in the Kelvin-Voigt model:

$$\Phi = \frac{1}{2}EA\eta\int_{l_0}^{l_1}\left(\frac{\partial^2 u_1}{\partial x_1\,\partial t}\right)^2 dx_1 + \frac{1}{2}EA\eta\int_{l_2}^{l_3}\left(\frac{\partial^2 u_2}{\partial x_2\,\partial t}\right)^2 dx_2 \quad (12)$$

where: η is the viscosity coefficient of the rope material according to the Kelvin-Voigt model

*) *Discretization of the elastic rope*: Using the Ritz-Galerkin expansion, the strain is expressed as:

$$u_1(x_1,t) = \sum_{i=1}^{N_1} X_{1i}(x_1)p_{1i}(t)\,;u_2(x_2,t) = \sum_{j=1}^{N_1} X_{2j}(x_2)p_{2j}(t) \quad (13)$$

where: $X_{1i}(x_1)$and $X_{2i}(x_2)$ are functions dependent on the boundary conditions, known as mode functions (or eigenfunctions); $p_1(t)$and$p_2(t)$are the solutions of the dynamic response, which are the generalized coordinates of the strain and need to be determined. Using the Galerkin expansion (or Galerkin method) with the boundary conditions, we obtain:

$$X_{1i}(x_1) = \sin\left(\frac{\pi(2i-1)}{2}\frac{x_1}{l_1}\right);\ X_{2j}(x_2) = \sin\left(\frac{\pi(2j-1)}{2}\frac{x_2}{l_2}\right) \quad (14)$$

*) At the initial moment of static equilibrium, let L_1 be the length of the rope, L_2 the length of the equilibrium rope, $l_{i0}(i = 1-4)$ and the length of the rope branches. We have:

$$l_{01} + l_{02} + \pi R = L_1; l_{03} + l_{04} + \pi R = L_2; l_{01} + l_{03} = l_{02} + l_{04} \quad (15)$$

*) Differential Equation of Motion. The generalized coordinate of the system is the angular displacement ϕ of the hoist, and the elastic generalized coordinates q_{1i}, q_{2j}. Using the Lagrange's equation, which has the form:

$$\frac{d}{dt}\left(\frac{\partial T}{\partial \dot{s}_i}\right) - \frac{\partial T}{\partial s_i} = -\frac{\partial U}{\partial s_i} - \frac{\partial \Phi}{\partial \dot{s}_i} + Q_i \quad (16)$$

where: $\boldsymbol{s} = \left[\phi p_{11}p_{12}\ldots p_{1N_1}p_{21}p_{22}\ldots p_{2N_2}\right]^T$, $U = U_E + U_G$.

Substituting the expressions from (7) to (12) into Equation 16 we obtain the system of differential equations of motion of the mechanism including the equation of ϕ, the equation of $p_{1i}$and the equation of p_{2i}as follows [25]:

$$\boldsymbol{M}(\boldsymbol{s})\ddot{\boldsymbol{s}} + \boldsymbol{C}(\boldsymbol{s},\dot{\boldsymbol{s}})\dot{\boldsymbol{s}} + \boldsymbol{g}(\boldsymbol{s}) = \boldsymbol{q} \tag{17}$$

where:

$$T = \frac{1}{2}\dot{\boldsymbol{s}}^T\boldsymbol{M}(\boldsymbol{s})\dot{\boldsymbol{s}};\ \boldsymbol{C}(\boldsymbol{s},\dot{\boldsymbol{s}}) = \frac{\partial \boldsymbol{M}(\boldsymbol{s})}{\partial \boldsymbol{s}}(\boldsymbol{E}_n \otimes \dot{\boldsymbol{s}}) - \frac{1}{2}\left(\frac{\partial \boldsymbol{M}(\boldsymbol{s})}{\partial \boldsymbol{s}}(\dot{\boldsymbol{s}} \otimes \boldsymbol{E}_n)\right)^T;\ \boldsymbol{g}(\boldsymbol{s}) = \left(\frac{\partial U}{\partial \boldsymbol{s}}\right)^T$$

$$\boldsymbol{q} = \left[(M_a - M_f)0\ldots0\right]^T_{1+N_1+N_2}$$

Equations 17 are written explicitly as in the Appendix. The derived general differential equations describe both the basic motion of the mechanism and the elastic motion of the rope. This elastic motion affects positional accuracy and induces vibrations in the lifting–lowering mechanism during operation. On the basis of the established model, control measures can be implemented to reduce the mechanism oscillations.

DYNAMIC ANALYSIS

- The motion profile of the lifting machine is shown in Figure 2, which follows a constant-acceleration law. In this profile, the start-up time is T_{on}, the shutdown time is T_{off}, and the uniform running time is T_s.
- Calculation parameter [16] – the mass of the empty cabins $m_0 = 39500\,kg$; material mass $m = 20000\,kg$, $m_1 = m_0 + m$, $m_2 = m_0$; the longitudinal stiffness of the rope EA = 1.5246×10^8 N/m; mass distribution r_b = 10.48 kg/m, r_c = 7.86 kg/m, hoist diameter D = 4.5 m, The mass of the hoist (flywheel type) is 4345 kg. The tensile strength of the cable is 900 kN. The maximum depth is 960 m.

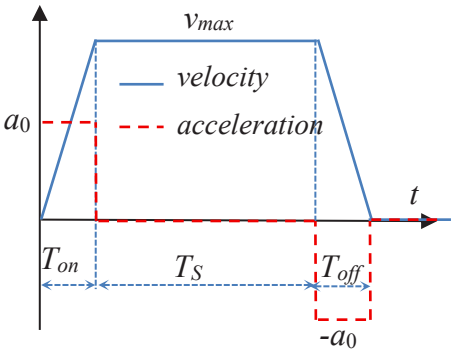

Figure 2. The motion law of the cabin

Case Study 1: The calculations for Case Study 1 are performed with Cabin 1 fully loaded, moving from a depth of 930 m to 30 m, while Cabin 2 is unloaded. The motion follows a constant-acceleration law, as shown in Figure 2, with a maximum speed of v_{max} = 9.31 m/s, constant acceleration a_0 = 0.7 m/s^2. From the law of motion, the time to turn on and off the machine can be determined as $T_{on} = T_{off}$ = 13.3 s. The calculated deformation of Cabin 1 cable branch is compared with its static deformation. The static deformation is determined as follows (Figure 3): Consider a tensioned cable model with length L, axial stiffness EA, subjected to a uniformly distributed load q (the rope's weight) and a concentrated force P.

Vertical force: $N(x) = P + q(L - x)$

Stress and strain: $\sigma(x) = \frac{N(x)}{A};\ \varepsilon(x) = \frac{\sigma(x)}{E}$

Vertical displacement at x: $u(x) = \int_0^x \varepsilon(s)ds = \frac{1}{EA}\left(Px + q\left(Lx - \frac{x^2}{2}\right)\right)$

Total elongation: $u(L) = \frac{1}{EA}(PL + qL^2/2)$

where: $P = m_1 g + g\rho_b l_3, L = l_1, q = g\rho_c$

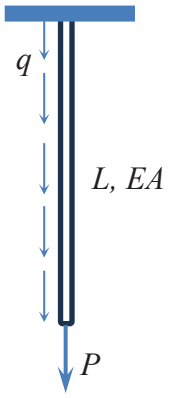

Figure 3. Static deformation of rope

CALCULATION RESULTS

Conditions for calculating numbers:

The initial conditions are set assuming that the system starts from rest (zero initial velocity), and the initial deformation corresponds to the static elongation of the rope. The governing equations are integrated using a time step of $\Delta t = 10^{-6}$ s, which ensures a numerical accuracy on the order of 10^{-3}.

Previous studies employing the Ritz-Galerkin method have shown that the deformation energy is concentrated primarily in the fundamental mode and decreases rapidly as the modal order

increases. Accordingly, the literature generally recommends retaining only the first mode when very high accuracy is not required, or the first three modes when a more refined approximation is desired, while the use of more than five modes is seldom reported. For this reason, and to reduce computational complexity while maintaining acceptable accuracy, the present study adopts the fundamental-mode truncation, i.e., $N_1 = N_2 = 1$.

The results of Case Study 1 clearly reveal the characteristic dynamic behavior of the hoisting rope in deep-shaft systems. As the conveyance accelerates according to the prescribed constant-acceleration profile, the effective working length of Rope Branch 1 changes significantly, generating pronounced transient elastic oscillations superimposed on the static elongation. Figure 4 illustrates the time-dependent movement of Rope Branch 1 during the acceleration and constant-velocity stages. The curve reflects the combined effect of static elongation and transient elastic oscillations generated when the hoisting system starts moving. This movement profile serves as the basis for subsequent analysis of elongation, deformation velocity, and vibrational behavior of the distributed-mass rope. As it is shown in Figure 5, the total elongation reaches a maximum of 4.58 m at approximately $t = 1.75$ s, which is fully consistent with the rapid increase in tensile force during the start-up phase. At this instant, the total elongation of 4.58 m over a rope length of 929 m corresponds to a relative axial strain of 0.49%, while the quasi-static component (3.85 m) corresponds to 0.41%. Steel wire ropes are known to accommodate elastic axial strains in the range of 0.3–0.6%, and in some industrial specifications up to approximately 0.8%, owing to the untwisting-retwisting deformation mechanism of their strands. The computed strain levels therefore remain within the expected elastic range for hoisting ropes and are considered realistic under deep-shaft operating conditions.

The maximum vibration amplitude occurs during the transition phase from acceleration to constant-speed motion and is approximately 0.95 m (defined as the maximum distance measured from the trough to the peak within one vibration cycle), gradually decreasing as the rope length shortens. This behavior reflects the inherent properties of a distributed-mass viscoelastic rope, the effective stiffness and modal characteristics of which vary with the instantaneous rope length. From a structural perspective, the corresponding axial strain remains within the elastic range of steel wire ropes. However, in practical deep-shaft operations, such large transient oscillations may still compromise operational safety. Consequently, mitigation measures – such as increasing damping through rope guides or damping devices, and implementing operational control strategies that limit transient speed ranges or adjust hoisting sequences

Figure 6–8 further illustrate the evolution of deformation velocity, highlighting the stronger oscillatory response during the early stage of hoisting when both inertia and tension variations peak. The numerical solution demonstrates the natural decay of these oscillations in the

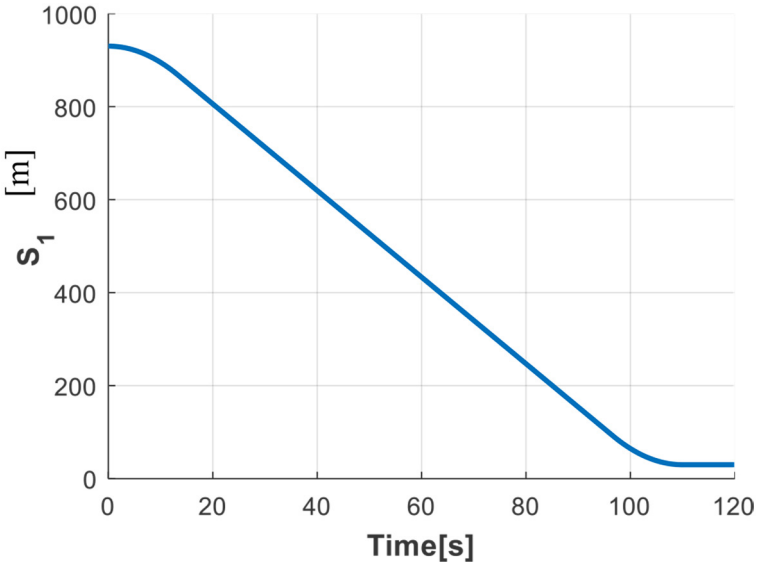

Figure 4. Movement of rope Branch 1

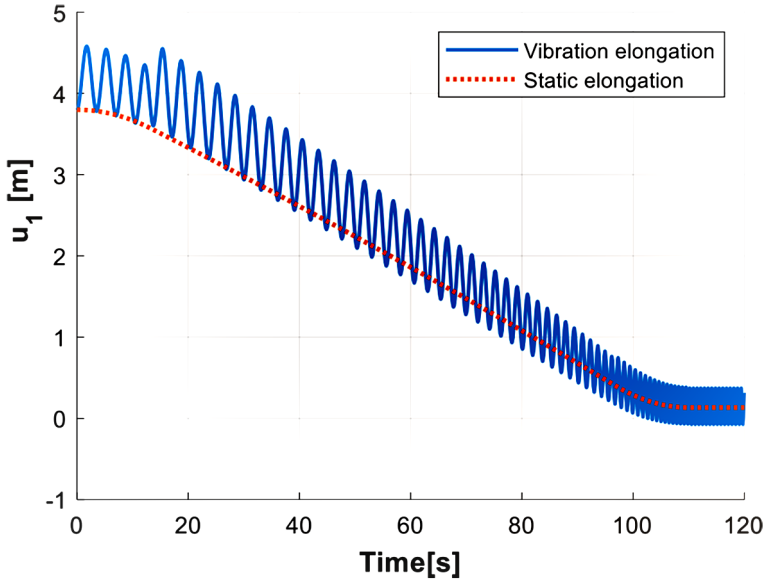

Figure 5. Overall elongation of rope Branch 1

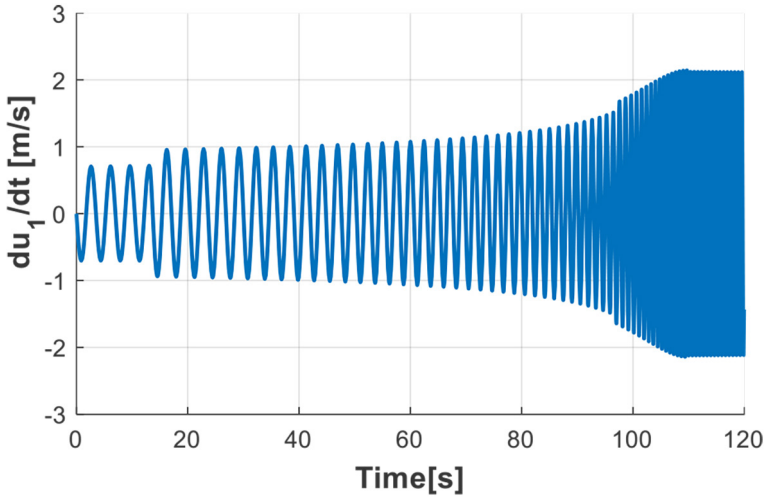

Figure 6. Deformation velocity of rope Branch 1

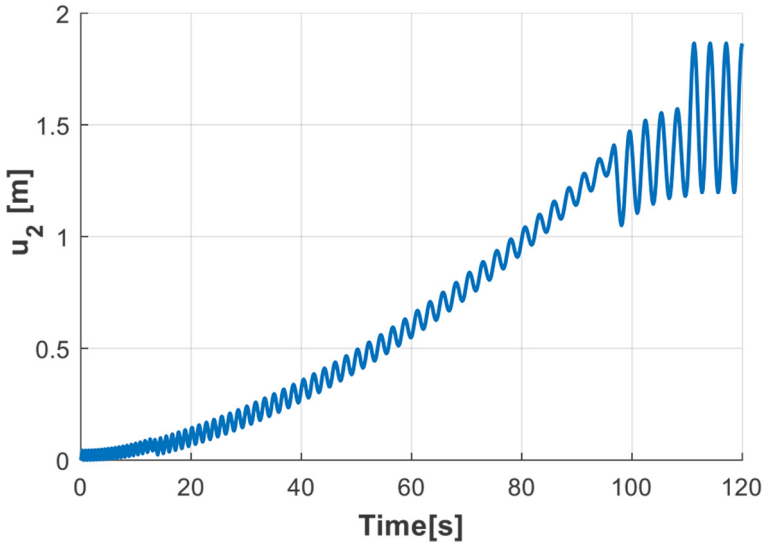

Figure 7. Overall elongation of rope counterweight 2

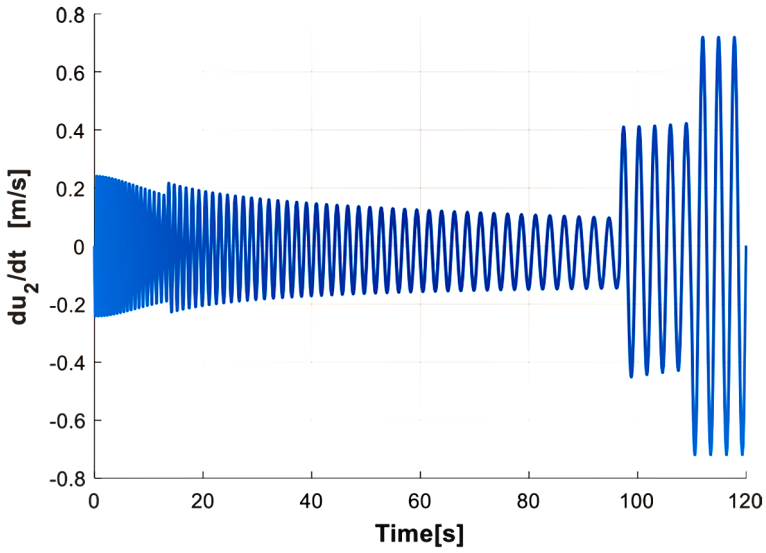

Figure 8. Deformation velocity of rope counterweight 2

undamped model, confirming that the discrete distributed-mass representation accurately captures the physical response of real hoisting ropes. The results validate the modeling approach, showing that the adopted segmentation method and Lagrangian formulation successfully reproduce both the magnitude and temporal evolution of rope dynamics.

The most significant implication of this case study is that elastic oscillations of the rope are substantial and cannot be neglected in deep-shaft hoisting analysis. Classical models that treat the rope as massless or apply quasi-static assumptions are unable to reproduce oscillation amplitudes approaching 1 m, as observed here. These large transient strains have direct consequences for control performance, dynamic loading of the drum and conveyance, and long-term fatigue of the rope. Furthermore, the findings emphasize that rope elongation and vibration are strongly dependent on the imposed velocity profile, suggesting that optimized acceleration–deceleration strategies are essential for mitigating dynamic fluctuations and enhancing operational safety in ultra-deep hoisting systems.

To further examine the influence of rope distributed mass on the predicted dynamic response, the results obtained from the full distributed-mass formulation were compared with those of a simplified model in which the distributed mass is neglected. As it is shown in Figure 9, notable discrepancies arise even under the same operating conditions. At $t = 1.75$ s the simplified model predicts an overall rope elongation of 3.94 m, whereas the distributed-mass model yields 4.58 m, corresponding to a relative difference of approximately 16.2%. This deviation is substantial and demonstrates that the distributed inertia of the rope plays a key role in accurately capturing both the vibration and static components of elongation.

Although the present study emphasizes displacement and velocity, acceleration characteristics are also highly relevant for assessing overloads, fatigue risk, and operational safety. Acceleration responses may serve as a sensitive diagnostic indicator for predicting excessive dynamic loading in hoisting components. Incorporating acceleration analysis into future numerical simulations will provide deeper insight into the strength-related behavior of long hoisting ropes.

Case Study 2: In this study, the parameters are the same as in the previous case. The damping coefficients are usually taken from about 0.1% to several percent of the stiffness coefficient, depending on the material and deformation type. Therefore, this study selected two values to investigate: $h = 0.001$ s^{-1} (0.1% of the stiffness coefficient) and $h = 0.005$ s^{-1} (0.5% of the stiffness coefficient). The result is as shown in Figures 10 and 11.

The results of Case Study 2 demonstrate that introducing viscous damping into the rope model effectively suppresses elastic oscillations in deep-shaft hoisting systems. As it is shown in Figure 10, even small damping coefficients significantly reduce the vibration amplitude around the static elongation and accelerate the decay of transient

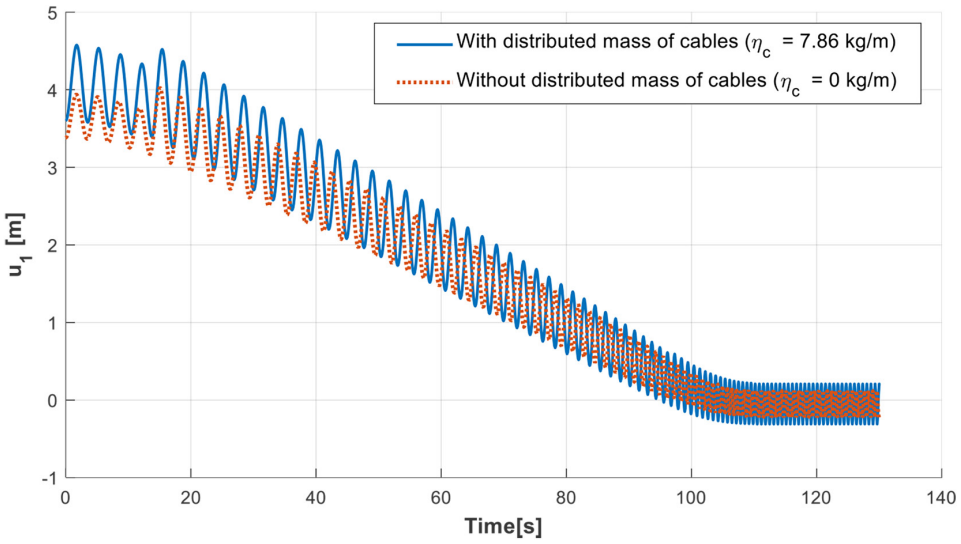

Figure 9. Overall elongation of rope Branch 1 when with and without distributed mass

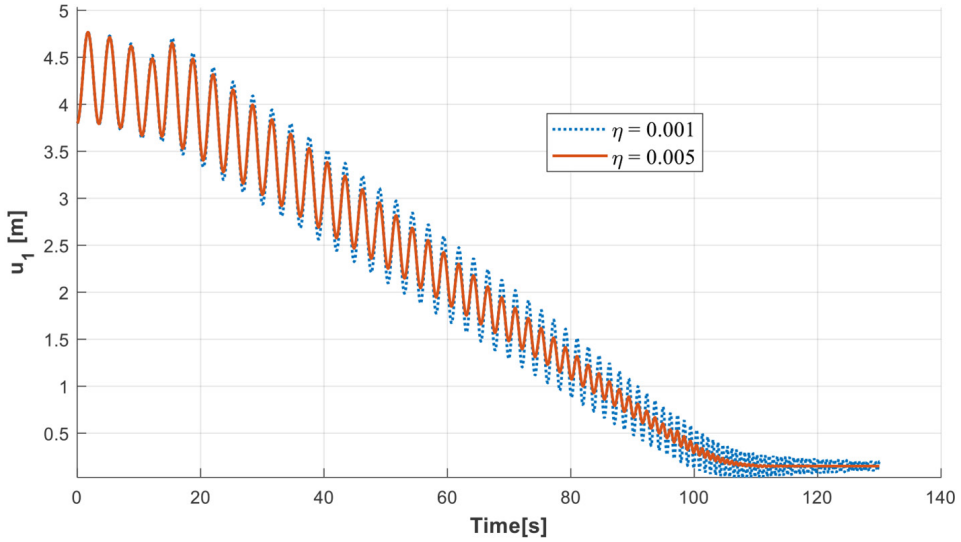

Figure 10. Overall elongation of rope Branch 1 with damping

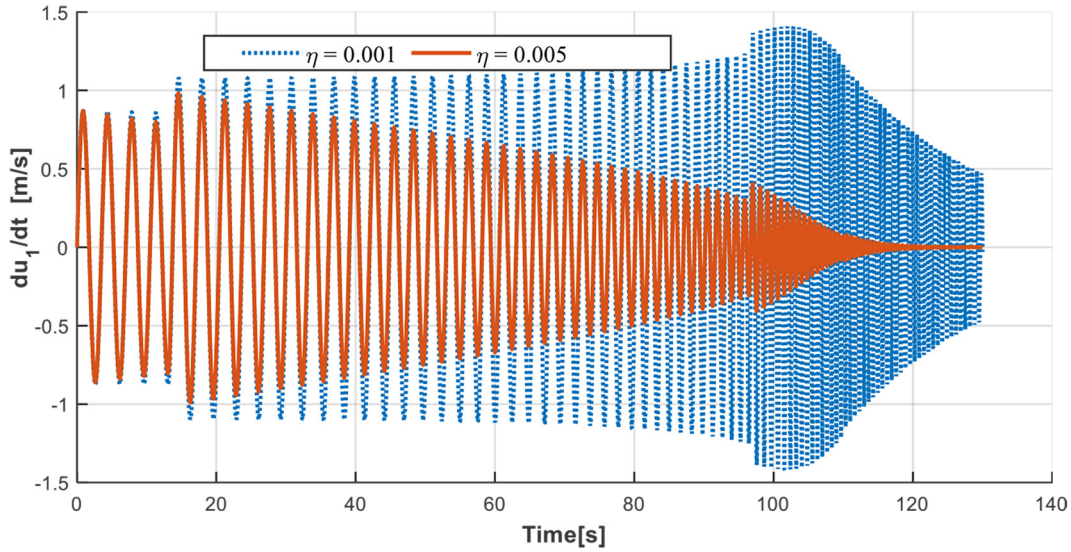

Figure 11. Deformation velocity of rope Branch 1

responses. This indicates that a modest level of damping is sufficient to control axial vibrations in long hoisting ropes. Figure 11 further highlights the attenuation of deformation velocity: the oscillatory envelope becomes progressively narrower compared to the undamped case, especially when $h = 0.005$ s^{-1}. The system reaches a stable state more rapidly, reducing dynamic loads acting on the conveyance, counterweight, and drum during the hoisting cycle.

The key implication is that viscous damping plays an essential role in enhancing the dynamic stability and safety of deep mine hoisting systems. The distributed-mass viscoelastic model accurately captures the vibration-decay characteristics, confirming its suitability for predicting real operational behavior. These findings suggest that optimized rope materials, lubrication conditions, and speed profiles can further mitigate vibration, prolong cable life, and improve the safety of ultra-deep shaft operations.

Case Study 3: In case Study 1, a constant acceleration profile was used. In the present investigation, to evaluate the influence of acceleration shaping on the dynamic response, the acceleration is defined using a sine-function law as follows:

$$a_1 = \begin{cases} a_1 \sin\left(\dfrac{\pi}{T_{on}} t\right), & 0 \le t \le T_{on} \\ 0, & T_{on} < t \le T_{on} + T_S \\ -a_1 \sin\left(\dfrac{\pi}{T_{on}} t\right), & T_{on} + T_S < t \le T_{on} + T_S + T_{off} \end{cases} \tag{18}$$

Using the same velocity and hoisting-duration conditions as in Case Study 1, the amplitude of the sine acceleration is computed as:

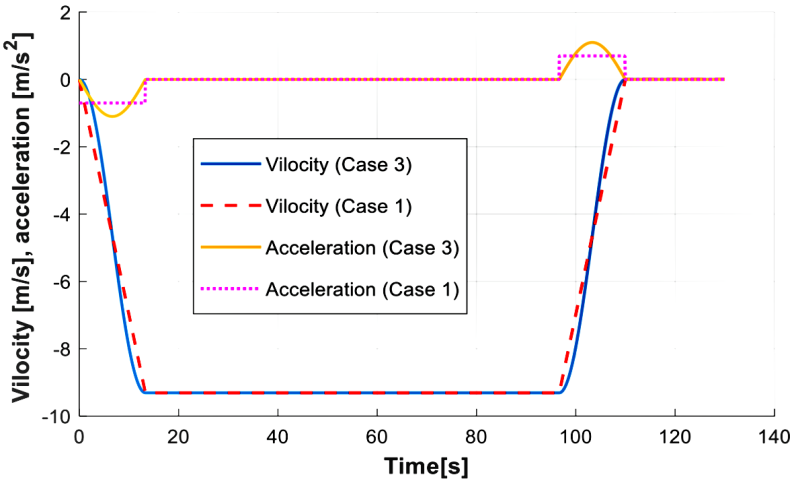

Figure 12. Velocity and acceleration curves

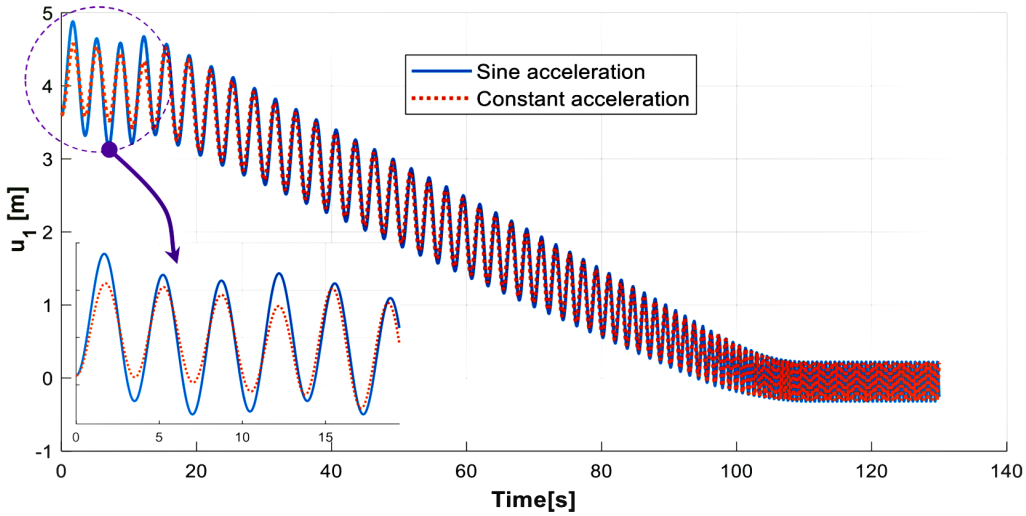

Figure 13. Overall elongation of rope Branch 1 dependent on acceleration

$$a_1 = \frac{\pi a_0}{2} = 1.01\,\mathrm{m/s^2}$$

where: a_0 is constant acceleration.

Figure 12 shows the resulting velocity and acceleration curves. With the calculation parameters taken as in case 1, the calculation results are shown in Figure 13, showing that the maximum overall elongation is about 4.89 m at t = 1.70 s. The maximum amplitude of deformation oscillation is about 1.46 m. Thus, the oscillation in the acceleration region ($0 < t < T_{on}$) increases significantly (about 6.8% compared to the case of constant acceleration). The elastic oscillation in this case is also more regular and there is no phenomenon of sudden increase in amplitude when changing phase in the case of constant acceleration. However, in this case, the maximum amplitude of oscillation increases greatly compared to the case of constant acceleration (0.95 m, an increase of about 53%). These findings demonstrate that the choice of acceleration profile has a strong influence on the transient response of deep hoisting systems.

CONCLUSIONS

This study developed a comprehensive dynamic model for deep mine hoisting systems that simultaneously considers rope elasticity, distributed mass, and viscoelastic damping – factors that are increasingly dominant as hoisting depths approach several hundred to nearly one thousand meters. The present model discretizes the rope into segments with distributed mass connected by weightless viscoelastic elements, enabling accurate representation of both static deformation and transient axial vibrations under operational loading. The full equations of motion were formulated using Lagrange's method combined with a Galerkin-type approximation to capture the elastic modes of the rope, resulting in a nonlinear equations system governing the dynamics of the drum, rope, cabin, and counterweight.

Simulation results demonstrate that the proposed model effectively reproduces characteristic dynamic behaviors observed in deep-shaft hoisting operations. In the first case study, where the system operates without damping, the rope experiences substantial elastic oscillations superimposed on a static elongation of up to 4.58 m, with initial vibration amplitudes reaching approximately 0.95 m.

These oscillations arise from rapid tension variations during the acceleration phase and diminish as the rope length shortens, reflecting the inherent modal properties of a distributed-mass tensile system.

The second case study highlights the essential role of viscous damping. Introducing small damping coefficients significantly reduces vibration amplitude and accelerates decay of deformation velocity, leading the system to stabilize more rapidly. This demonstrates that material damping, lubrication conditions, or engineered damping components can substantially improve dynamic stability and reduce dynamic loading on the drum, hoisting ropes, and conveyance.

The approach enables accurate prediction of rope deformation, vibration levels, and their dependence on operational parameters such as velocity profiles and rope length. These insights establish a solid basis for optimizing hoisting control strategies, improving structural safety, reducing fatigue of wire ropes, and providing information about the design of next-generation deep mine hoisting systems.

Future research may extend this work by incorporating torsional-axial coupling, guide-rail interactions, multi-cable friction effects, and active vibration suppression schemes to further enhance the predictive capability and applicability of the model in ultra-deep mining environments. In addition, experimental validation using accelerometers installed on operating mine hoists should be pursued. Such measurements would allow direct comparison between the predicted acceleration responses and the actual dynamic behavior, providing a robust foundation for model calibration and subsequent analytical refinement

Acknowledgment

This research is funded by Hanoi University of Civil Engineering (HUCE) under grant number 34-2025/KHXD-TĐ.

REFERENCES

1. Reutov, A., Kobishchanov, V. and Sakalo, V. Dynamic modeling of lift hoisting mechanism block pulley. Procedia Engineering, 2016; 150: 1303–1310.
2. Ilin, S., et al., Influence of dynamic processes in mine hoists on safety of exploitation of shafts with broken geometry. Scientific Bulletin of the National Mining University, 2016; 3: 48–53.

3. Ilin, S., et al. Control of technical state of mine hoisting installations. in E3S Web of Conferences. 2020. EDP Sciences.
4. Shebela, Z. and Pavelek, D. Investigation of hoisting system dynamics. Issledovanie dinamiki podemnykh ustanovok. 1988.
5. Ilin, S., et al., Risk-forming dynamic processes in units of mine hoists of vertical shafts. Scientific Bulletin of the National Mining University, 2018; 5: 64–71.
6. Kaczmarczyk, S. and Ostachowicz, W. Transient vibration phenomena in deep mine hoisting cables. Part 2: Numerical simulation of the dynamic response. Journal of Sound and Vibration, 2003; 262(2): 245–289.
7. Ma, Y. and Xiao, X. Dynamic analyses of hoisting ropes in a multi-rope friction mine hoist and determination of proper hoisting parameters. Journal of Vibroengineering, 2016; 18(5): 2801–2817.
8. Chaplin, C., Hoisting ropes for drum winders- the mechanics of degradation. Mining Technology, 1994; 76(877): 213–219.
9. Khoreshok, A., Tyulenev, M. and Vöth, S. Conditions for Minimum Dynamic Loading of Multi-brake Hoists. in 8th Russian-Chinese Symposium Coal in the 21st Century: Mining, Processing, Safety. 2016. Atlantis Press.
10. Zhang, J., et al., Dynamic torsional characteristics of mine hoisting rope and its internal spiral components. Tribology International, 2017; 109: 182–191.
11. Yao, J., et al., Investigation of dynamic load in superdeep mine hoisting systems induced by drum winding. Shock and Vibration, 2021; 1: 4756813.
12. Wang, G., Xiao, X. and Liu, Y. Dynamic modeling and analysis of a mine hoisting system with constant length and variable length. Mathematical Problems in Engineering, 2019; 1: 4185362.
13. Cao, G., et al., Dynamic response of parallel hoisting system under drive deviation between ropes with time-varying length. Shock and Vibration, 2017; 2017(1): 6837697.
14. Wolny, S. and Matachowski, F. Analysis of loads and stresses in structural elements of hoisting installations in mines. Engineering Transactions, 2010; 58(3–4): 153–174.
15. Kaczmarczyk, S. and Ostachowicz, W. Transient vibration phenomena in deep mine hoisting cables. Part 1: Mathematical model. Journal of Sound and Vibration, 2003; 262(2): 219–244.
16. Yao, J. and Xiao, X. Effect of hoisting load on transverse vibrations of hoisting catenaries in floor type multirope friction mine hoists. Shock and Vibration, 2016; 1: 8598749.
17. Wang, J., et al., Lateral response of cable-guided hoisting system with time-varying length: theoretical model and dynamics simulation verification. Proceedings of the Institution of Mechanical Engineers, Part C: Journal of Mechanical Engineering Science, 2015. 229(16): 2908–2920.
18. Yao, J., Deng, Y. and Xiao, X. Optimization of hoisting parameters in a multi-rope friction mine hoist based on the multi-source coupled vibration characteristics of hoisting catenaries. Advances in Mechanical Engineering, 2017; 9(3): 1687814017693216.
19. Lu, H., Peng, Y., Cao, S., Zhu, Z. Parameter sensitivity analysis and probabilistic optimal design for the main-shaft device of a mine hoist. Arabian Journal for Science and Engineering, 2019, 44: 971–979.
20. Guo, Y., Zhang, D., Zhang, X., Wang, S., Ma, W. Experimental study on the nonlinear dynamic characteristics of wire rope under periodic excitation in a friction hoist. Shock and Vibration, 2020; 1: 8506016.
21. Guo, Y., Zhang, D., Chen, K., Feng, C., Ge, S. Longitudinal dynamic characteristics of steel wire rope in a friction hoisting system and its coupling effect with friction transmission. Tribology International, 2018; 119: 731–743.
22. Peterka, P., Krešák, J. The causes of the damage to the bearing rope-failure analysis. Advances in Science and Technology Research Journal, 2018; 12(2): 231–236.
23. Peterka, P., Krešák, J., Vojtko, M. Experience of the crane steel wire ropes non-destructive tests. Advances in Science and Technology Research Journal, 2018; 12(4): 157–163.
24. Kalentev, E., Vaclav, S., Božek, P., Tarasov, V., Korshunov, A. Numerical analysis of the stress-strain state of a rope strand. Advances in Science and Technology Research Journal, 2017; 11(2), 231–239.
25. Shabana, A. A. Dynamics of Multibody Systems. Cambridge: Cambridge University Press. 2020.